Modified Fronsdal coordinates for maximally extended Schwarzschild spacetime

Andrei Galiautdinov*
Department of Physics and Astronomy, University of Georgia, Athens, Georgia 30602, USA
(Dated: October 9, 2025)

We introduce a coordinate system that complements the Kruskal–Szekeres extension. Like the standard construction, it covers the maximally extended Schwarzschild manifold in its entirety, while offering an additional advantage of expressing the areal radius as an explicit function of the new coordinates. Its main limitation, however, is that radial null geodesics are no longer represented as 45-degree lines in the Kruskal plane, making the causal structure more difficult to interpret. Nevertheless, the new system offers a compelling aesthetic trade-off: among all known maximally extended systems—including those of Kruskal–Szekeres, Israel, Fronsdal, Novikov, and Synge—it exhibits the highest degree of symmetry with respect to Schwarzschild's original r- and t-coordinate lines. It trades the regular pattern of Kruskal's light cones for a symmetric nesting arrangement of the two-dimensional spheres. The proposed extension sheds new light on the closely related Fronsdal's six-dimensional embedding construction, and clarifies the deep connection that exists between the most important implicit (Kruskal-Szekeres) and explicit (Israel's) procedures for maximal extension of the Schwarzschild geometry that is well known to those working in the field but rarely presented in textbooks on general relativity.

I. INTRODUCTION

The celebrated Kruskal-Szekeres procedure [1, 2] for maximal extension of the Schwarzschild vacuum,[1]

$$ds^2 = \frac{4r_s^3}{r} e^{-r/r_s} \left(dT^2 - dX^2\right) - r^2 d\Omega^2, \quad d\Omega^2 \equiv d\theta^2 + \sin^2\theta\, d\varphi^2, \tag{1}$$

has its physical origins in Penrose's form [3, 4],

$$v = t + \left(r + r_s \ln\left|\frac{r}{r_s} - 1\right|\right), \quad u = t - \left(r + r_s \ln\left|\frac{r}{r_s} - 1\right|\right), \tag{2}$$

of the Eddington-Finkelstein (EF) coordinates [5, 6]. The intimate connection between the two systems, (T, X) and (v, u), was clearly elaborated in Ref. [7] by Misner, Thorne, and Wheeler, which undoubtedly helped both systems gain their tremendous popularity. The principal advantage of the Kruskal-Szekeres and other related doubly-null coordinates is that they always represent radial null rays as 45-degree lines in the Kruskal plane, making the causal structure of the underlying spacetime manifold immediately apparent.

For almost seventy years, the Kruskal–Szekeres extension has played a central role in general relativistic research. Its elegance, simplicity, and mathematical beauty have created a lasting legacy in the field, unlikely to be surpassed by any other extension system. Despite its enduring importance, however, the system has one notable drawback: it expresses the areal radius, r, through a pair of transcendental equations,

$$e^{r/r_s}\left(\frac{r}{r_s} - 1\right) = X^2 - T^2, \tag{3}$$

and

$$\frac{t}{2r_s} = \begin{cases} \operatorname{arctanh}\left(\frac{T}{X}\right), & r > r_s, \\ \operatorname{arctanh}\left(\frac{X}{T}\right), & r < r_s, \end{cases} \tag{4}$$

*Electronic address: ag1@uga.edu

[1] Here we use the notation common in the educational literature on general relativity: ds^2 denotes the spacetime metric (line element, or interval), (T, X) are the Kruskal–Szekeres coordinates, r is the areal radius, t is the Schwarzschild time measured by distant observers, (θ, φ) are the standard angular coordinates on the 2-sphere, and $r_s = 2M$ is the Schwarzschild radius, with M the mass of the black hole expressed in geometrized units (meters). The areal radius r is defined such that a 2-sphere labeled by r has surface area $4\pi r^2$; in general it does not coincide with the proper radial distance from any center—indeed, a center may not even exist in the spacetime (as in the case of a wormhole).

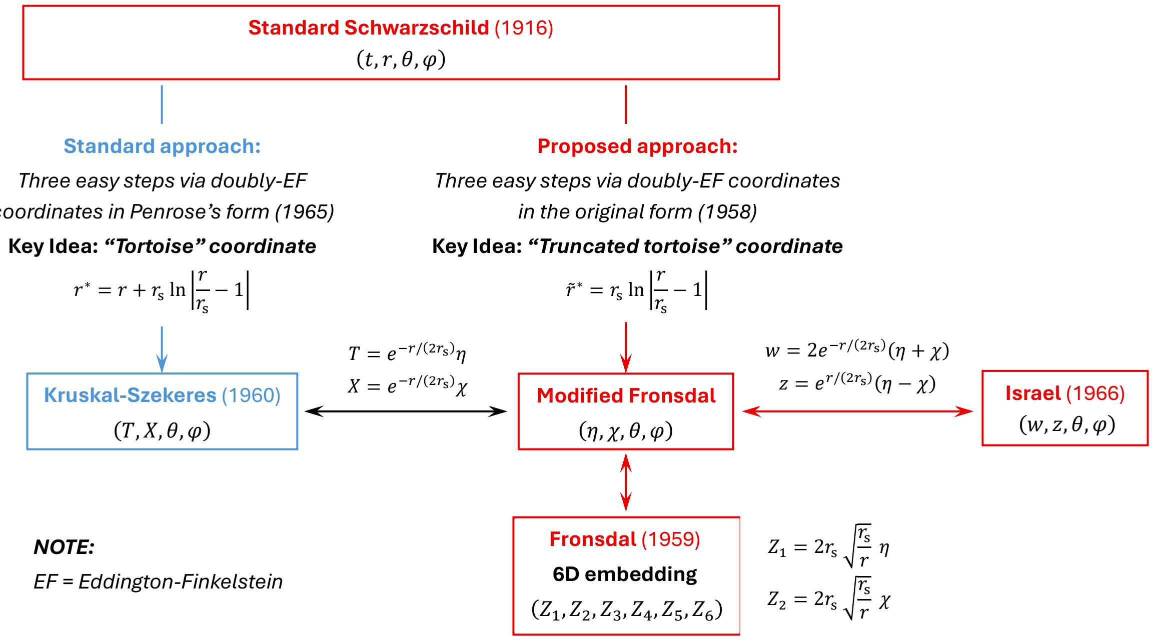

FIG. 1: (Color online) Flowchart showing the relations among most important explicit (red) and implicit (blue) extension systems. The asymmetry of Israel's spacetime diagram (as depicted in Fig. 1 in Ref. [8]) is due to the opposing signs of the exponents appearing in the corresponding transformation equations. Generalization to other systems may be implemented via $r^*_{\text{general}} = f(r) + r_s \ln\left|\frac{r}{r_s} - 1\right|$ (however, see Sec. V for a simpler method).

which prevents the metric coefficients from being written explicitly in terms of the adopted coordinates (T, X). As a result, even routine computations, such as finding Christoffel symbols or curvature components, are beset with significant technical difficulties. This affects not only research but also how the subject is typically taught. While black holes and the Kruskal–Szekeres extension are routinely presented in general relativity courses, no other maximally extended system is usually introduced. Consequently, students who may be knowledgeable in the causal structure of black holes often find themselves unable to perform concrete, explicit analytical calculations, particularly those describing physics on the extended spacetime manifold. While we cannot reliably predict the direction in which observational research will take us tomorrow, a solid grounding in maximal extensions may one day become increasingly important, especially if more exotic objects, such as white holes, must eventually be taken into account. The following presentation is written with these considerations in mind and is intended, in part, to help bridge this gap in the training of students aiming to conduct creative research in general relativity.

The above, then, naturally raises the question: Can one construct an alternative, explicit coordinate system that likewise exhibits a compelling symmetry while also being suitable for practical calculations?

It is evident from Eq. (3) that the main complication arises from the exponential prefactor. Therefore, the most straightforward approach would be to redefine the standard Kruskal-Szekeres coordinates so that this exponent is eliminated. This can be done quite easily, essentially by inspection. Readers who prefer this simplified approach may consult the flowchart in Fig. 1 (as well as Table I), and then proceed directly to our main equations, (18)-(21), and Section V.

For readers interested in a step-by-step construction starting from Schwarzschild's original metric, we will offer a different strategy. We will retrace the usual sequence of transformations familiar from the standard Kruskal–Szekeres procedure, but with one important modification: instead of using the full radial tortoise coordinate,[2] we will use its truncated version, as per Eddington and Finkelstein's original proposal. This will allow us to carry out each step in a fully transparent and explicit manner, making the relationships between successive forms of the metric easy to understand. What we will essentially propose here is an alternative path to the maximally extended Schwarzschild

[2] The name comes from the singular transformation of the areal coordinate r (see the chart in Fig. 1), which includes a logarithmically stretching contribution. This ingeniously chosen contribution allows the metaphorical tortoise to finally reach (and cross into!) the black hole (whereas in Schwarzschild coordinates the infalling photon geodesics appear stuck just outside of the horizon).

TABLE I: Areal radius, r, in various coordinate systems considered in this article.

Schwarzschild (t, r, θ, φ)	**Kruskal-Szekeres** (T, X, θ, φ)	**Israel** (w, z, θ, φ)	**Fronsdal** $(Z_1, Z_2, Z_3, Z_4, Z_5, Z_6)$	**Modified Fronsdal** $(\eta, \chi, \theta, \varphi)$
r	$e^{r/r_\mathrm{s}}\left(\frac{r}{r_\mathrm{s}}-1\right)=X^2-T^2$	$\frac{r}{r_\mathrm{s}}-1=-\frac{wz}{2}$	$\frac{r}{r_\mathrm{s}}=\left(1-\frac{Z_2^2-Z_1^2}{4r_\mathrm{s}^2}\right)^{-1}$	$\frac{r}{r_\mathrm{s}}-1=\chi^2-\eta^2$

spacetime, which may be regarded as complementary to the traditional Kruskal-Szekeres formulation.

Before proceeding, let us interject a relevant historical remark.

One interesting explicit form of the maximally extended Schwarzschild metric was proposed by Israel in 1966 [8] (also, [9–11]). Israel's line element,

$$ds^2 = r_\mathrm{s}^2\left(2dwdz - \frac{r_\mathrm{s}}{r}z^2dw^2\right) - r^2d\Omega^2, \quad \frac{r}{r_\mathrm{s}} = 1-\frac{wz}{2}, \tag{5}$$

was based solely on the ingoing Eddington-Finkelstein coordinates,[3] which resulted in a highly asymmetric spacetime description. The pronounced lopsidedness of the corresponding spacetime diagram (as in Fig. 1 in Ref. [8]) may have contributed to the reasons why Israel's important work did not receive the widespread attention it rightfully deserves. With this in mind, our approach can also be viewed as an attempt to symmetrize—and, in doing so, popularize—Israel's extension by incorporating, in addition to the ingoing coordinates, the outgoing coordinates as well. What emerges from this "symmetrizing" construction is a four-dimensional line element that ties together all three historically important maximal extensions: the Kruskal-Szekeres implicit system, Israel's explicit but asymmetric system, and the elegant, yet somewhat mysterious, six-dimensional pseudo-Euclidean isometric embedding of the Schwarzschild spacetime,

$$ds^2 = dZ_1^2 - dZ_2^2 - dZ_3^2 - dZ_4^2 - dZ_5^2 - dZ_6^2, \tag{6}$$

introduced by Fronsdal in 1959 [12]. It is therefore rather surprising that our metric (Eqs. (17) and (18) below) does not appear to have been previously written down or actually used. There were two early indications—in the well-known papers by Rindler [13] and Synge [14])—suggesting what such a metric might look like. Apart from these, the only other work that touches upon the subject seems to be a recent pedagogical note by Unruh [15], in which a different approach to Fronsdal's embedding is briefly discussed.

In the pages that follow, we will refer to the new metric as the modified Fronsdal extension. This name is appropriate because the final transformation (22) leading from our coordinates to those used by Fronsdal is remarkably simple, highlighting the direct algebraic relationship between the two. Our construction will preserve the essential geometric insight of Fronsdal's original approach while reformulating it in a fully four-dimensional form. Unlike the original embedding, which requires six ambient dimensions and primarily serves as a geometric existence proof, our metric is immediately usable for calculations within the intrinsic spacetime. In this sense, our extension offers a streamlined and pedagogically transparent realization of essentially the same idea, thereby justifying the proposed terminology.

II. THE METRIC

Our detailed, physically motivated derivation of the modified Fronsdal extension for Schwarzschild geometry proceeds as follows.

Combining the original ingoing and outgoing Eddington-Finkelstein coordinates $(\tilde v, \tilde u)$ [5, 6],

$$\tilde v = t + r_\mathrm{s}\ln\left|\frac{r}{r_\mathrm{s}}-1\right|, \quad \tilde u = t - r_\mathrm{s}\ln\left|\frac{r}{r_\mathrm{s}}-1\right|, \quad t = (\tilde v+\tilde u)/2, \quad r/r_\mathrm{s} = \begin{cases} 1+e^{(\tilde v-\tilde u)/(2r_\mathrm{s})}, & r>r_\mathrm{s}, \\ 1-e^{(\tilde v-\tilde u)/(2r_\mathrm{s})}, & r<r_\mathrm{s}, \end{cases} \tag{7}$$

with

$$d\tilde v = dt + \frac{r_\mathrm{s}}{r}\frac{dr}{1-\frac{r_\mathrm{s}}{r}}, \quad d\tilde u = dt - \frac{r_\mathrm{s}}{r}\frac{dr}{1-\frac{r_\mathrm{s}}{r}}, \tag{8}$$

---

[3] The connection is exhibited by $e^{v/(2r_\mathrm{s})} = w/2$, $r/r_\mathrm{s} = 1-wz/2$, with $dv = 2r_\mathrm{s}dw/w$, $dr = -(r_\mathrm{s}/2)(wdz+zdw)$, which upon substitution into the ingoing EF metric, $ds^2 = (1-r_\mathrm{s}/r)\,dv^2 - 2dvdr - r^2d\Omega^2$, produces Eq. (5).

we first convert the standard Schwarzschild line element,

$$ds^2 = \left(1 - \frac{r_\mathrm{s}}{r}\right) dt^2 - \frac{dr^2}{1 - \frac{r_\mathrm{s}}{r}} - r^2 d\Omega^2, \tag{9}$$

to

$$ds^2 = \frac{1}{4}\left(1 - \frac{r_\mathrm{s}}{r}\right)\left[(d\tilde{v} + d\tilde{u})^2 - \left(\frac{r}{r_\mathrm{s}}\right)^2 (d\tilde{v} - d\tilde{u})^2\right] - r^2 d\Omega^2. \tag{10}$$

This step eliminates the most troubling metric coefficient g_{rr}, but places $r = r_\mathrm{s}$ at $\tilde{v} - \tilde{u} = -\infty$.[4] To bring the horizon back from coordinate infinity, we employ the re-scaling trick [16, 17],

$$\tilde{V} = e^{\tilde{v}/(2r_\mathrm{s})}, \quad \tilde{U} = \mp e^{-\tilde{u}/(2r_\mathrm{s})}, \quad d\tilde{v} = 2r_\mathrm{s} d\tilde{V}/V, \quad d\tilde{u} = -2r_\mathrm{s} d\tilde{U}/\tilde{U}, \tag{11}$$

with $\mp$ referring to $r > r_\mathrm{s}$ and $r < r_\mathrm{s}$, respectively, which gives

$$\tilde{V}\tilde{U} = -\frac{r}{r_\mathrm{s}}\left(1 - \frac{r_\mathrm{s}}{r}\right), \quad r > 0, \tag{12}$$

valid for any r. This allows elimination of the prefactor $(1 - r_\mathrm{s}/r)$ in (10), leading to

$$ds^2 = r_\mathrm{s}^2 \left[2\left(\frac{r}{r_\mathrm{s}} + \frac{r_\mathrm{s}}{r}\right) d\tilde{V} d\tilde{U} - \left(1 + \frac{r_\mathrm{s}}{r}\right)\left(\tilde{U}^2 d\tilde{V}^2 + \tilde{V}^2 d\tilde{U}^2\right)\right] - r^2 d\Omega^2, \tag{13}$$

where

$$r/r_\mathrm{s} = 1 - \tilde{V}\tilde{U}, \quad e^{t/r_\mathrm{s}} = \mp\tilde{V}/\tilde{U}. \tag{14}$$

The resulting metric may be viewed as the symmetrized version of Israel's line element introduced in Ref. [8] (also see some interesting discussions in Refs. [18–22].) This can be seen by exhibiting the transformation equations linking the two systems,

$$w = 2e^{r/(2r_\mathrm{s})}\tilde{V}, \quad z = e^{-r/(2r_\mathrm{s})}\tilde{U}, \tag{15}$$

which, after some algebra, recovers Eq. (5). Notice that it is the presence of the opposite signs in the exponents in (15) which makes Israel's spacetime diagram distinctly asymmetric (compare to (21) in the Kruskal case below). Finally, an additional coordinate transformation,

$$\tilde{V} = \eta + \chi, \quad \tilde{U} = \eta - \chi, \tag{16}$$

brings the metric to the form,

$$ds^2 = \frac{4r_\mathrm{s}^3}{r}\left\{\left[1 - \eta^2\left(1 + \frac{r}{r_\mathrm{s}}\right)\right] d\eta^2 + 2\eta\chi\left(1 + \frac{r}{r_\mathrm{s}}\right) d\eta d\chi - \left[1 + \chi^2\left(1 + \frac{r}{r_\mathrm{s}}\right)\right] d\chi^2\right\} - r^2 d\Omega^2, \tag{17}$$

or, somewhat more compactly,

$$ds^2 = \frac{4r_\mathrm{s}^3}{r}\left[d\eta^2 - d\chi^2 - \left(1 + \frac{r}{r_\mathrm{s}}\right)(\eta d\eta - \chi d\chi)^2\right] - r^2 d\Omega^2, \tag{18}$$

where

$$\frac{r}{r_\mathrm{s}} = 1 + \chi^2 - \eta^2, \quad \frac{t}{2r_\mathrm{s}} = \begin{cases} \operatorname{arctanh}\left(\frac{\eta}{\chi}\right), & r > r_\mathrm{s}, \\ \operatorname{arctanh}\left(\frac{\chi}{\eta}\right), & r < r_\mathrm{s}, \end{cases} \tag{19}$$

---

[4] Which corresponds to setting $e^{(\tilde{v}-\tilde{u})/(2r_\mathrm{s})} = 0$ in Eq. (7).

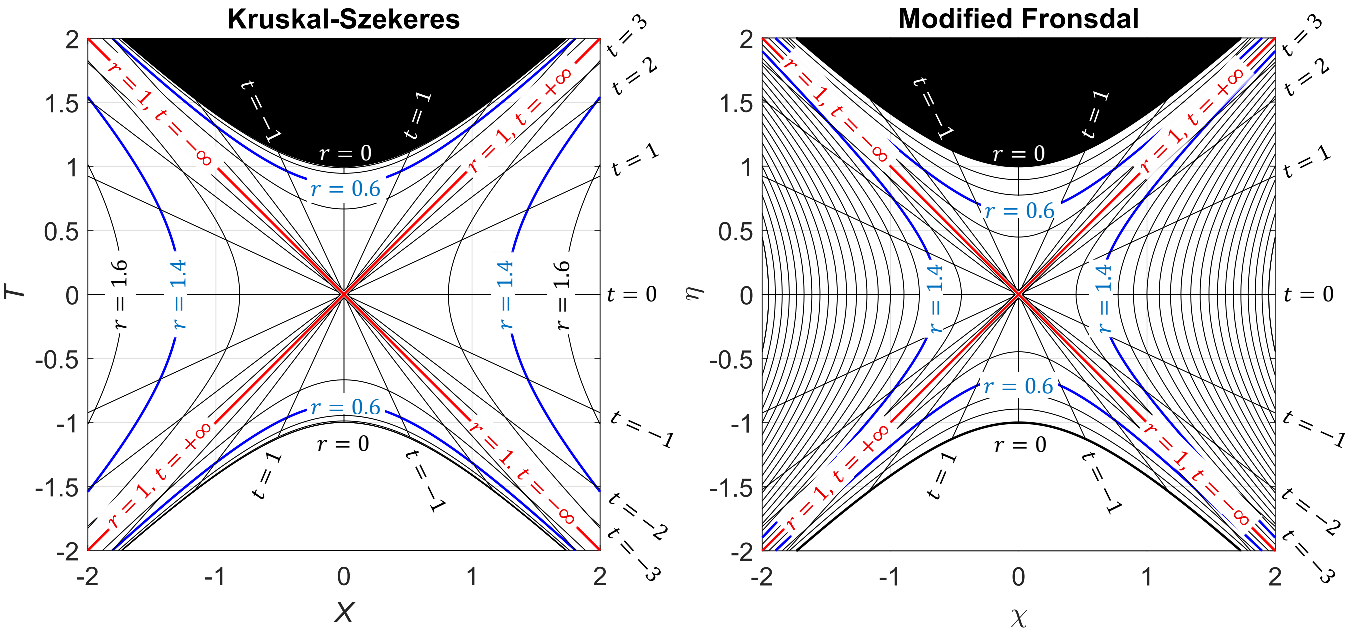

FIG. 2: (Color online) Comparison of the Kruskal and modified Fronsdal diagrams. Each point in either diagram represents a two-dimensional sphere of areal radius r. The $r =$ constant lines are plotted in steps of $0.2\,r_\mathrm{s}$ and form hyperbolas in both cases. The factor r_s on the labels of curves is omitted for clarity. To emphasize the enhanced symmetry of the modified Fronsdal diagram, a representative pair of curves is highlighted in blue color ($r = 0.6\,r_\mathrm{s}$ and $1.4\,r_\mathrm{s}$), while the remaining $r =$ constant curves are shown in black. Straight lines of constant t passing through the origin are plotted for $t/r_\mathrm{s} = -\infty, -3, -2, -1, 0, 1, 2, 3, \infty$, with the red lines representing the white and black hole horizons ($r = r_\mathrm{s}$, $t = \pm\infty$). The usual Kruskal–Szekeres coordinates (T, X) are related to the modified Fronsdal coordinates (η, χ) via Eq. (21), preserving the ratio $T/X = \eta/\chi$.

which should be compared to Eqs. (3) and (4), and

$$r > r_\mathrm{s}: \begin{cases} \eta = \left|\frac{r}{r_\mathrm{s}} - 1\right|^{1/2} \sinh\left(\frac{t}{2r_\mathrm{s}}\right), \\ \chi = \left|\frac{r}{r_\mathrm{s}} - 1\right|^{1/2} \cosh\left(\frac{t}{2r_\mathrm{s}}\right), \end{cases} \qquad r < r_\mathrm{s}: \begin{cases} \eta = \left|\frac{r}{r_\mathrm{s}} - 1\right|^{1/2} \cosh\left(\frac{t}{2r_\mathrm{s}}\right), \\ \chi = \left|\frac{r}{r_\mathrm{s}} - 1\right|^{1/2} \sinh\left(\frac{t}{2r_\mathrm{s}}\right), \end{cases} \tag{20}$$

where both branches of the square root must be taken into account.

This indicates a simple connection between Kruskal's original and the modified coordinates,

$$T = e^{r/(2r_\mathrm{s})}\eta, \quad X = e^{r/(2r_\mathrm{s})}\chi, \tag{21}$$

which will be exploited in what follows. The six-dimensional isometric embedding is then immediately recovered by introducing the Fronsdal coordinates via

$$Z_1 = 2r_\mathrm{s}\sqrt{\frac{r_\mathrm{s}}{r}}\,\eta, \quad Z_2 = 2r_\mathrm{s}\sqrt{\frac{r_\mathrm{s}}{r}}\,\chi, \tag{22}$$

and

$$Z_3 = \int^r \sqrt{\frac{r_\mathrm{s}}{r} + \frac{r_\mathrm{s}^2}{r^2} + \frac{r_\mathrm{s}^3}{r^3}}\,dr, \quad Z_4 = r\sin\theta\cos\varphi, \quad Z_5 = r\sin\theta\sin\varphi, \quad Z_6 = r\cos\theta, \tag{23}$$

with

$$r = \frac{r_\mathrm{s}}{1 - \frac{Z_2^2 - Z_1^2}{4r_\mathrm{s}^2}} = \sqrt{Z_4^2 + Z_5^2 + Z_6^2}, \tag{24}$$

in terms of which the line element assumes the famed pseudo-Euclidean form (6). One may appreciate how naturally the transformation equations (22) and (23) defining Fronsdal's embedding have emerged in our derivation (cf. Ref. [12]; also [23]).

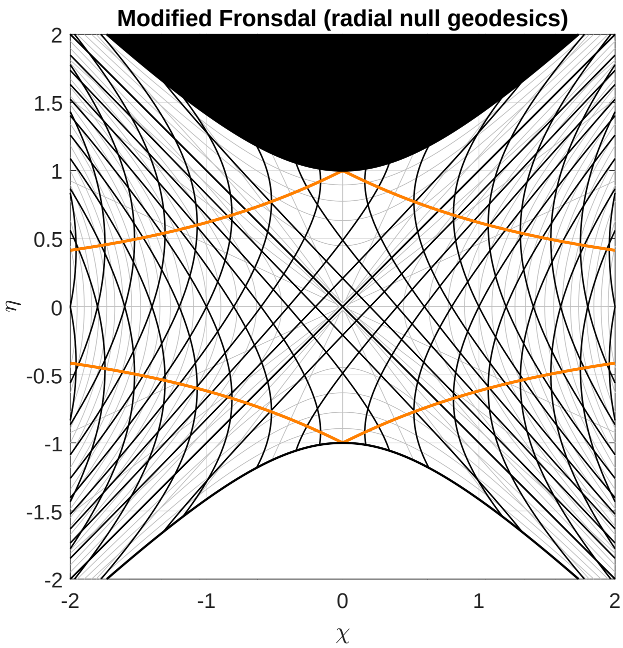

FIG. 3: (Color online) Radial null geodesics (black curves) in modified Fronsdal coordinates plotted on the basis of Eq. (25), where χ_0 varies in steps of 0.2. The meaning of the curves plotted in orange is elaborated upon in Sec. III C. Notice characteristic Finkelsteinian collapse of the light cones as they approach the singularity. Compare to the light-cone structure depicted in Fig. 2 of Fronsdal's original paper [12].

The spacetime diagram corresponding to (19) is depicted in Fig. 1 (right panel). Notice that in our extension the constant-t lines of the original Schwarzschild geometry, unlike in Israel's, are straight, passing through the origin, and are similar to Kruskal's. The constant-r lines are also beautifully distributed, forming a highly symmetric nesting arrangement surrounding the horizon (cf. Gullstrand-Painlevé-type extensions recently discussed in Ref. [24]; also [16] and [15]).

III. THE CAUSAL STRUCTURE

A. Radial Null geodesics

In the modified Fronsdal coordinates, (η, χ), the ingoing and outgoing radial null geodesics (plotted in Fig. 3) are described by the equation,

$$\eta \pm \chi = C e^{(\eta^2 - \chi^2)/2}, \quad C = \chi_0 e^{\chi_0^2/2}, \tag{25}$$

where χ_0 is the value of the χ coordinate at $\eta = 0$. This may be seen most easily by differentiating (21),

$$dT/dX = \mp 1 = (\eta + 2r_{\mathrm{s}}\, d\eta/dr) \,/\, (\chi + 2r_{\mathrm{s}}\, d\chi/dr)\,, \tag{26}$$

whose solution is

$$\eta \pm \chi = \tilde{C} e^{-r/(2r_{\mathrm{s}})}, \tag{27}$$

which is equivalent to (25) on the basis of (19).

B. Gullstrand-Painlevé "raindrops"

By Gullstrand-Painlevé raindrops we mean a collection of point-like massive probes radially infalling from rest at spatial infinity. In modified Fronsdal geometry, the corresponding infalling timelike geodesics are described by the

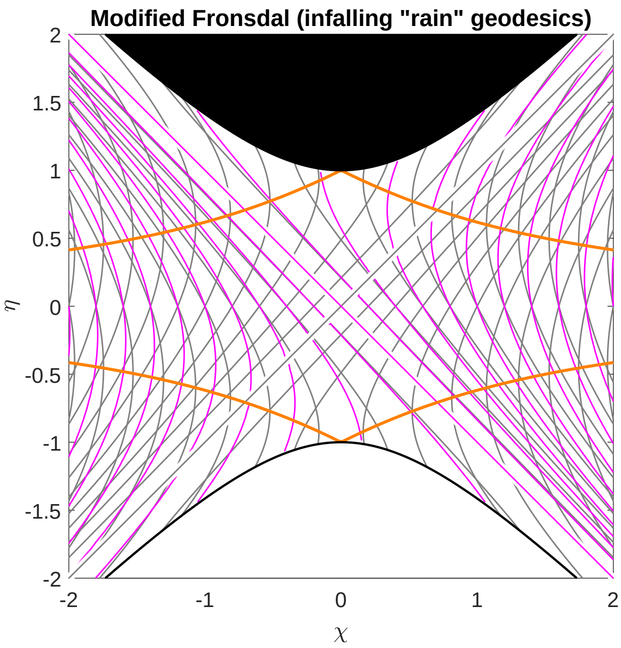

FIG. 4: (Color online) Infalling Gullstrand-Painlevé geodesics (magenta curves) superimposed on radial null geodesics (light gray curves) plotted on the basis of Eq. (29), where χ_0 varies in steps of 0.2.

equation,

$$\frac{d\eta}{d\chi} = \frac{\chi\,(r/r_{\rm s})^{3/2} - \eta}{\eta\,(r/r_{\rm s})^{3/2} - \chi}, \tag{28}$$

or,

$$\frac{\eta+\chi}{\eta-\chi} = \mp C\left|\frac{(r/r_{\rm s})^{1/2}+1}{(r/r_{\rm s})^{1/2}-1}\right| \exp\left\{-\left[\frac{2}{3}\left(\frac{r}{r_{\rm s}}\right)^{3/2} + 2\left(\frac{r}{r_{\rm s}}\right)^{1/2}\right]\right\}, \quad \frac{r}{r_{\rm s}} = 1+\chi^2-\eta^2, \tag{29}$$

where

$$C = \left|\frac{(r_0/r_{\rm s})^{1/2}-1}{(r_0/r_{\rm s})^{1/2}+1}\right| \exp\left\{\frac{2}{3}\left(\frac{r_0}{r_{\rm s}}\right)^{3/2} + 2\left(\frac{r_0}{r_{\rm s}}\right)^{1/2}\right\}, \quad \frac{r_0}{r_{\rm s}} = 1+\chi_0^2, \tag{30}$$

with $\mp$ referring to $r > r_{\rm s}$ and $r < r_{\rm s}$, respectively. In the above, χ_0 is the value of the χ-coordinate at $\eta = 0$ (see Fig. 4). The proof (left as a straightforward exercise) of Eqs. (28) and (29) boils down to rewriting various well known results pertaining to radially infalling geodesics of the standard Schwarzschild metric in terms of the newly introduced coordinates (η, χ). The extended solution then, in addition, automatically describes the motion of the (formally regarded as infalling) "raindrops" that come to rest at the spatial infinity of the "other" universe after being emitted by the past singularity (white hole).

C. The nature of the constant-η and constant-χ hypersurfaces

Referring back to Fig. (3), let us take a closer look at the central, diamond-shaped region bounded by the curves plotted in orange. These particular curves are singled out because they are defined by the condition

$$\eta = \pm\frac{1}{\sqrt{1+\frac{r}{r_{\rm s}}}}, \tag{31}$$

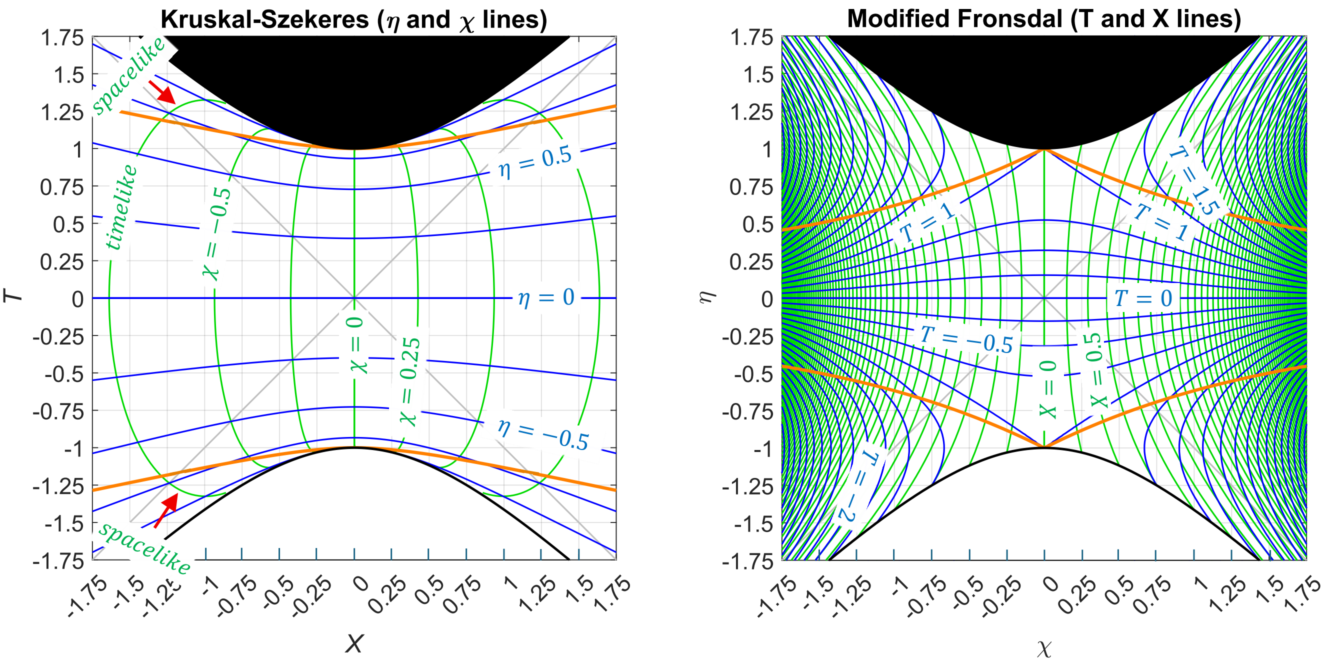

FIG. 5: (Color online) Left panel: the constant-η (blue) and constant-χ (green) lines in the Kruskal-Szekeres coordinates (T, X). Right panel: Kruskal's constant-T (blue) and constant-X (green) lines in the modified Fronsdal coordinates (η, χ). Compare to Figs. 1 and 2 in Ref. [16] and Fig. 2 in Ref. [15].

or, equivalently,

$$\eta = \pm\sqrt{1 + \frac{\chi^2}{2} - \sqrt{\chi^2\left(1 + \frac{\chi^2}{4}\right)}}, \tag{32}$$

which correspond precisely to the loci where $g_{00} = 0$. In other words, they mark the transition between timelike and spacelike behavior of the η-lines (of constant χ) and pass through the "turning points" of various null geodesics. Within this region,

$$g_{00} = \frac{4r_s^3}{r}\left[1 - \eta^2\left(1 + \frac{r}{r_s}\right)\right] d\eta^2 > 0 \quad \text{(positive)}, \tag{33}$$

which implies that the bounded segments of η-lines threading the diamond are timelike and may be interpreted as the worldlines of certain temporarily existing, physically realizable, accelerated (except for the central one) local observers. Outside this region, the η-lines are spacelike (tachyonic) and therefore cannot be associated with physical observers.

These considerations prompt us to re-draw the η- and χ-lines, as well as the diamond itself, in the original Kruskal plane. Note that the diamond's boundary is now described by

$$1 + e^{-|X/T|}\left(X^2 - T^2\right) = \pm\frac{X}{T}, \tag{34}$$

which follows from Eqs. (31), (21), and (3). The results are depicted in Fig. 5 (left panel), where, for completeness, we have also included the reciprocal plot showing the T- and X-lines in (η, χ) coordinates (right panel).

Notice again that each of the η-lines (lines of constant χ) consists of a central timelike segment contained within the diamond, flanked by spacelike segments on either side. These outer portions, when represented in the original Kruskal plane, appear to extend backward in the Kruskal time coordinate T, making their spacelike character particularly evident (cf. the cases of Gullstrand-Painlevé in Ref. [16] and Synge in Ref. [15]).

In addition, the χ-lines (lines of constant η) provide a natural slicing of the spacetime into spacelike hypersurfaces. This foliation will serve as a useful tool in the next section, where we examine the dynamical interpretation of the Schwarzschild wormhole.

IV. APPLICATION TO WORMHOLE DYNAMICS

Let us now apply Eq. (17) to the Einstein–Rosen bridge [25], also known as the Schwarzschild wormhole. The classic analysis by Fuller and Wheeler [26] employs Kruskal's implicit coordinate system, which makes the description rather elaborate. While their treatment has become a standard reference in the literature and reveals many essential features of the wormhole's geometry, the associated spacetime foliation—based on the auxiliary parameter $\gamma = T/(4{+}X^2)^{1/2}$—was, by their own admission, "quite arbitrarily selected." Although mathematically consistent, this slicing does not arise naturally from the coordinates themselves and appears somewhat artificial. In contrast, our approach uses an explicit coordinate system, in which the foliation by constant-η hypersurfaces (the χ-lines) emerges directly from the geometry and provides a more transparent, coordinate-adapted setup for analyzing wormhole dynamics. In this sense, the proposed approach complements the classic treatment by offering an alternative, geometrically motivated framework for exploring wormhole dynamics.

Referring to Eq. (17), we see that at any fixed η, the wormhole's spatial geometry is described by the line element

$$d\ell^2 = \frac{4r_\mathrm{s}^3}{r}\left[1+\chi^2\left(1+\frac{r}{r_\mathrm{s}}\right)\right]d\chi^2 + r^2 d\Omega^2, \tag{35}$$

with

$$\chi^2 = \frac{r}{r_\mathrm{s}} - 1 + \eta^2, \qquad 2\chi\, d\chi = \frac{dr}{r_\mathrm{s}}, \qquad d\chi^2 = \frac{dr^2}{4r_\mathrm{s}^2\chi^2}.$$

Its Flamm embedding in Euclidean space [27],

$$d\ell^2 = dr^2 + dZ^2 + r^2 d\Omega^2, \tag{36}$$

is therefore given by

$$dZ^2 = \frac{1+\eta^2/\rho}{\rho - 1 + \eta^2}\, dr^2, \qquad \rho \equiv \frac{r}{r_\mathrm{s}}, \tag{37}$$

or, equivalently,[5]

$$\frac{Z}{r_\mathrm{s}} = \pm\int_{\rho_0}^{\rho} \sqrt{\frac{1+\chi^2/\xi}{\xi - 1 + \eta^2}}\, d\xi, \qquad \rho_0 = \begin{cases} 1-\eta^2, & 0 \le |\eta| < 1, \\ 0, & |\eta| > 1, \end{cases} \tag{38}$$

whose η-dependent profiles are plotted in Fig. 6 and Fig. 7 (cf., e.g., Ref. [28] and the more recent Ref. [29]).

Notice that for η such that $0 \le |\eta| < 1$, Eq. (38) may be written in the alternative form

$$0 \le |\eta| < 1: \quad \frac{Z}{r_\mathrm{s}} = \pm 2\left[\sqrt{(\rho - 1 + \eta^2)\left(1 + \frac{\eta^2}{\rho}\right)} - \eta \int_{\eta/\sqrt{1-\eta^2}}^{\eta/\sqrt{\rho}} \sqrt{\frac{1 - \left(\frac{1}{\eta^2} - 1\right)\zeta^2}{1+\zeta^2}}\, d\zeta\right]. \tag{39}$$

If needed, the integral in square brackets may be expressed in terms of the hyperbolic version of the incomplete elliptic integral of the second kind,

$$\tilde{E}(\phi, k) \equiv \int_0^{\phi} \sqrt{1 - k^2 \sinh^2\psi}\, d\psi = \int_0^{\sinh\phi} \sqrt{\frac{1-k^2\zeta^2}{1+\zeta^2}}\, d\zeta. \tag{40}$$

Either way, at $\eta = 0$ we recover the standard result for the maximally open throat,

$$\eta = 0: \quad \frac{Z}{r_\mathrm{s}} = 2\sqrt{\frac{r}{r_\mathrm{s}} - 1}. \tag{41}$$

---

[5] Here, ρ_0 is chosen so that the minimal areal radius $\rho_0 \equiv r_\mathrm{min}/r_\mathrm{s}$ on each of the Flamm plots (Fig. 6 and Fig. 7) corresponds to $Z = 0$. For $|\eta| < 1$ (connected universes), the condition $dZ/dr = \pm\infty$, which defines r_min, then implies from Eq. (37) that $\rho_0 - 1 + \eta^2 = 0$, i.e., $\rho_0 = 1 - \eta^2$. For $|\eta| > 1$ (disconnected universes), we set $\rho_0 = 0$ to ensure that the integrand never becomes imaginary.

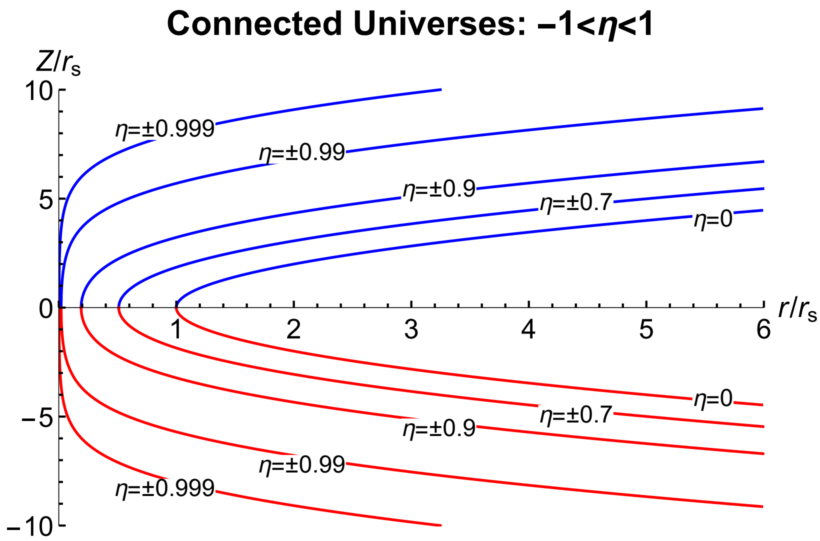

FIG. 6: (Color online) The η-dependent Flamm's embedding of Schwarzchild's wormhole as described by Eq. (38) for $0 \leq |\eta| < 1$. "Our" universe is depicted in blue (with $Z/r_s > 0$), the "other" universe is depicted in red (with $Z/r_s < 0$). The throat is maximally open at $\eta = 0$ ($r_{\rm throat} = r_s$).

The proof of Eq. (39) proceeds as follows.

Our strategy is to recast the integrand in (38) into a form that naturally separates into two contributions: one that is the exact differential of an algebraic term, and another that integrates to the elliptic-integral–like expression. First, observe that

$$\begin{aligned}\sqrt{\frac{1+\eta^2/\xi}{\xi-1+\eta^2}} &= \left[\sqrt{\frac{1+\eta^2/\xi}{\xi-1+\eta^2}} - \sqrt{\frac{\xi-1+\eta^2}{\xi+\eta^2}}\,\frac{\eta^2}{\xi^{3/2}}\right] + \sqrt{\frac{\xi-1+\eta^2}{\xi+\eta^2}}\,\frac{\eta^2}{\xi^{3/2}} \\ &= \left[\frac{1+\eta^2/\xi}{\sqrt{(\xi-1+\eta^2)(1+\eta^2/\xi)}} + \frac{(\xi-1+\eta^2)(-\eta^2/\xi^2)}{\sqrt{(\xi-1+\eta^2)(1+\eta^2/\xi)}}\right] \\ &\quad - \sqrt{\frac{1-\left(\frac{1}{\eta^2}-1\right)(-\eta/\xi^{1/2})^2}{1+(-\eta/\xi^{1/2})^2}}\left(-\frac{\eta^2}{\xi^{3/2}}\right). \end{aligned} \tag{42}$$

Next, consider differentials,

$$\begin{aligned} d\sqrt{(\xi-1+\eta^2)\left(1+\frac{\eta^2}{\xi}\right)} &= \frac{1}{2}\,\frac{d\left[(\xi-1+\eta^2)\left(1+\frac{\eta^2}{\xi}\right)\right]}{\sqrt{(\xi-1+\eta^2)\left(1+\frac{\eta^2}{\xi}\right)}} \\ &= \frac{1}{2}\left[\frac{1+\eta^2/\xi}{\sqrt{(\xi-1+\eta^2)(1+\eta^2/\xi)}} + \frac{(\xi-1+\eta^2)(-\eta^2/\xi^2)}{\sqrt{(\xi-1+\eta^2)(1+\eta^2/\xi)}}\right] d\xi, \end{aligned} \tag{43}$$

and

$$d\left(\frac{\eta}{\xi^{1/2}}\right) = -\frac{\eta}{2\xi^{3/2}}\,d\xi = \frac{1}{2\eta}\left(-\frac{\eta^2}{\xi^{3/2}}\right)d\xi, \tag{44}$$

where η is treated as constant. Finally, multiplying (42) by $d\xi$, taking into account (43) and (44), and integrating with the properly chosen limits, we obtain the desired decomposition, recovering Eq. (39).

Notice a somewhat peculiar way in which wormhole dynamics is described here. Due to our specific choice of spacetime slicing, the corresponding η-dependent embedding goes from being purely tachyonic (since the η-field is spacelike in the interval $-\infty < \eta < -1$, representing initially disconnected universes), to a mixure of timelike (for $0 < r/r_s < (1-\eta^2)/\eta^2$) and spacelike (for $r/r_s > (1-\eta^2)/\eta^2$) when η is restricted to the range $-1 < \eta < 1$ (the

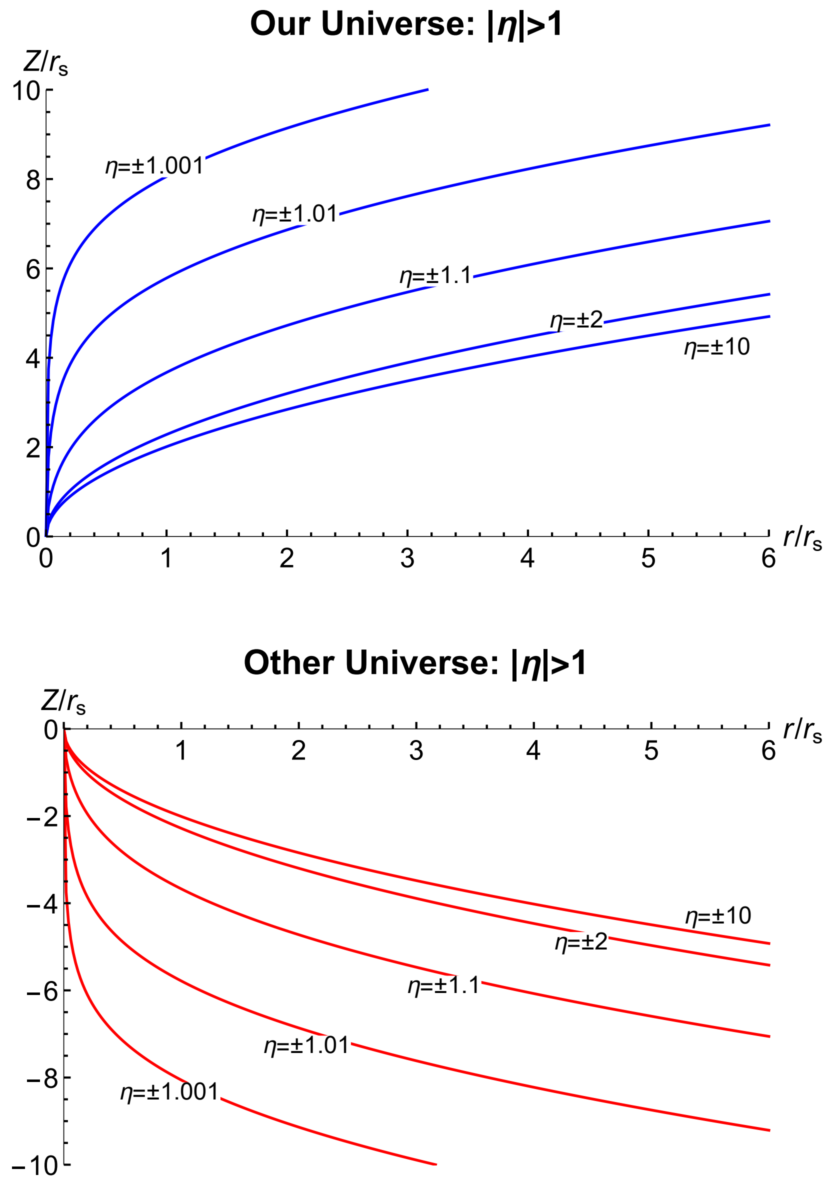

FIG. 7: (Color online) Evolution of the two disconnected universes at $|\eta| > 1$, as described by Eq. (38). Notice that the cusps of the corresponding embeddings settle on certain limiting shapes as $\eta \to \pm\infty$, which in this figure are virtually indistinguishable from those at $\eta = \pm 10$. The figure may give the misleading impression that the two disconnected universes touch at $Z = 0$, which is not the case. For $|\eta| > 1$, the universes are in fact spatially separated in the χ (or X) direction.

throat), and then back to purely tachyonic for $1 < \eta < +\infty$ (again corresponding to disconnected universes). In principle, this description is sufficient for the problem at hand, since the η and χ fields are never tangent to one another on the extended manifold.

V. SIMPLIFIED APPROACH

Let us now explore the simplified approach mentioned in the Introduction, which assumes familiarity with the standard Kruskal–Szekeres line element, Eq. (1). The key idea is to remove the exponential factor in the metric by introducing a compensating exponential in the coordinate transformation, Eq. (21), subject to

$$\frac{r}{r_s} = 1 + \chi^2 - \eta^2, \tag{45}$$

which guarantees that Eq. (3)—and, therefore, Einstein's field equations—are satisfied. This strategy is loosely analogous to the way a coordinate singularity in the metric can be canceled by a corresponding singularity in the transformation equations. The calculation then proceeds as follows:

From Eqs. (21) and (45) we get,

$$dT = \left(\frac{dr}{2r_{\rm s}}\eta + d\eta\right) e^{r/(2r_{\rm s})}, \quad dX = \left(\frac{dr}{2r_{\rm s}}\chi + d\chi\right) e^{r/(2r_{\rm s})}, \quad \frac{dr}{r_{\rm s}} = 2(\chi d\chi - \eta d\eta), \tag{46}$$

which after squaring gives,

$$dT^2 = \left(\frac{dr^2}{4r_{\rm s}^2}\eta^2 + \frac{\eta}{r_{\rm s}}d\eta dr + d\eta^2\right) e^{r/r_{\rm s}}, \quad dX^2 = \left(\frac{dr^2}{4r_{\rm s}^2}\chi^2 + \frac{\chi}{r_{\rm s}}d\chi dr + d\chi^2\right) e^{r/r_{\rm s}}, \quad \frac{dr^2}{4r_{\rm s}^2} = (\chi d\chi - \eta d\eta)^2. \tag{47}$$

Substituting into Eq. (1) produces (with the spherical part omitted for clarity),

$$\begin{aligned} ds^2 &= \frac{4r_{\rm s}^3}{r} e^{-r/r_{\rm s}} \left[(\eta^2 - \chi^2)\frac{dr^2}{4r_{\rm s}^2} + (\eta d\eta - \chi d\chi)\frac{dr}{r_{\rm s}} + d\eta^2 - d\chi^2\right] e^{+r/r_{\rm s}} \\ &= \frac{4r_{\rm s}^3}{r} \left[(\eta^2 - \chi^2)\frac{dr^2}{4r_{\rm s}^2} + (\eta d\eta - \chi d\chi)\frac{dr}{r_{\rm s}} + d\eta^2 - d\chi^2\right] \\ &= \frac{4r_{\rm s}^3}{r} \left[\left(1 - \frac{r}{r_{\rm s}}\right)(\eta d\eta - \chi d\chi)^2 - 2(\eta d\eta - \chi d\chi)^2 + d\eta^2 - d\chi^2\right] \\ &= \frac{4r_{\rm s}^3}{r} \left[-\left(1 + \frac{r}{r_{\rm s}}\right)(\eta d\eta - \chi d\chi)^2 + d\eta^2 - d\chi^2\right], \end{aligned} \tag{48}$$

which is the same as our main Eq. (18). Generalization may then be implemented via the transformation

$$T = e^{r/(2r_{\rm s})}\eta(x^0, x^1), \quad X = e^{r/(2r_{\rm s})}\chi(x^0, x^1), \tag{49}$$

subject to

$$r(x^0, x^1) = r_{\rm s}\left(1 + \chi^2 - \eta^2\right), \tag{50}$$

and

$$ds^2 = \frac{4r_{\rm s}^3}{r}\left[\left(\frac{dr}{2r_{\rm s}}\eta + d\eta\right)^2 - \left(\frac{dr}{2r_{\rm s}}\chi + d\chi\right)^2\right], \tag{51}$$

where η and χ are now regarded as arbitrary functions of the new coordinates x^0 and x^1. Eq. (50) again guarantees the validity of the Einstein field equations. In a sense, this simple yet unconventional procedure brings the playful challenge of creating maximal extensions directly into the classroom. With a suitable choice of the areal radius $r(x^0, x^1)$, a bit of patience, and a bit of luck, anyone can now construct their own beautiful maximal extension.

VI. CONCLUSIONS

We have presented a simple, physically motivated construction that provides further clarification of Fronsdal's original, historically important embedding of the maximally extended Schwarzschild manifold in a higher-dimensional pseudo-Euclidean space. Along the way, we proposed a modified, four-dimensional form of Fronsdal's metric, which may be viewed both as Israel's line element recast into a highly symmetrical form and, in a certain sense, as a dual and complementary reformulation of the standard Kruskal-Szekeres system. The main attractive features of the proposed extension are: (1) the explicit form of the transformation equations connecting it to standard Schwarzschild coordinates; (2) the explicit form of the areal radius and the resulting four-dimensional metric, which may prove useful for general relativistic calculations; and (3) the regular appearance of the corresponding spacetime representation diagram.

Despite having been frequently cited—especially during the early years of black hole research—Fronsdal's original work has not been widely adopted in educational literature on general relativity. This may be due to its formal and rather abstract nature, which tends to appeal more to mathematically oriented researchers in the field. In this pedagogical account, we have reformulated it as a concrete and more accessible alternative within a fully four-dimensional framework, which may be better suited for educational purposes, especially in situations where the emphasis is on explicit computations rather than on diagrammatic causal analysis.

Appendix A: Christoffel symbols and curvature

Here, for completeness, we list non-vanishing Christoffel symbols and curvature components associated with (17):

$$\Gamma^0_{00} = -\Gamma^1_{10} = \frac{\eta\left(\chi^2\left(1+\chi^2\right)-\left(1-\eta^2\right)^2\right)}{\left(r/r_{\mathrm{s}}\right)^3}, \quad \Gamma^0_{10} = -\Gamma^1_{11} = \frac{-\chi\left(\eta^2\left(1-\eta^2\right)+\left(1+\chi^2\right)^2\right)}{\left(r/r_{\mathrm{s}}\right)^3}, \tag{A1}$$

$$\Gamma^0_{11} = \frac{\eta\left(\eta^4-4\eta^2\chi^2-3\eta^2+3\chi^4+6\chi^2+3\right)}{\left(r/r_{\mathrm{s}}\right)^3}, \quad \Gamma^1_{00} = \frac{-\chi\left(3-6\eta^2+3\eta^4+3\chi^2-4\eta^2\chi^2+\chi^4\right)}{\left(r/r_{\mathrm{s}}\right)^3}, \tag{A2}$$

$$\Gamma^0_{22} = -\frac{\eta}{2}, \quad \Gamma^1_{22} = -\frac{\chi}{2}, \quad \Gamma^2_{12} = \Gamma^3_{13} = \frac{2\chi}{r/r_{\mathrm{s}}}, \quad \Gamma^2_{20} = \Gamma^3_{30} = \frac{-2\eta}{r/r_{\mathrm{s}}}, \tag{A3}$$

$$\Gamma^0_{33} = -\frac{1}{2}\eta\sin^2\theta, \quad \Gamma^1_{33} = -\frac{1}{2}\chi\sin^2\theta, \quad \Gamma^2_{33} = -\sin\theta\cos\theta, \quad \Gamma^3_{23} = \cot\theta, \tag{A4}$$

and

$$R^0_{001} = R^1_{110} = \frac{4\eta\chi\left(\eta^2-\chi^2-2\right)}{\left(r/r_{\mathrm{s}}\right)^4}, \tag{A5}$$

$$R^2_{102} = R^3_{103} = R^2_{012} = R^3_{013} = \frac{2\eta\chi\left(\eta^2-\chi^2-2\right)}{\left(r/r_{\mathrm{s}}\right)^4}, \tag{A6}$$

$$R^0_{101} = \frac{4\left(\chi^4-\left(\eta^2-2\right)\chi^2+1\right)}{\left(r/r_{\mathrm{s}}\right)^4}, \quad R^1_{001} = \frac{4\left(\eta^4-\eta^2\left(\chi^2+2\right)+1\right)}{\left(r/r_{\mathrm{s}}\right)^4}, \tag{A7}$$

$$R^2_{002} = R^3_{003} = \frac{-2\left(\eta^4-\eta^2\left(\chi^2+2\right)+1\right)}{\left(r/r_{\mathrm{s}}\right)^4}, \quad R^2_{121} = R^3_{131} = \frac{-2\left(\chi^4-\left(\eta^2-2\right)\chi^2+1\right)}{\left(r/r_{\mathrm{s}}\right)^4} \tag{A8}$$

$$R^0_{202} = R^1_{212} = \frac{-1}{2(r/r_{\mathrm{s}})}, \quad R^3_{232} = \frac{1}{r/r_{\mathrm{s}}}, \tag{A9}$$

$$R^0_{303} = R^1_{313} = \frac{-\sin^2\theta}{2(r/r_{\mathrm{s}})}, \quad R^2_{332} = \frac{-\sin^2\theta}{r/r_{\mathrm{s}}}, \tag{A10}$$

where $x^0 = \eta$, $x^1 = \chi$, $x^2 = \theta$, $x^3 = \varphi$, and $r/r_{\mathrm{s}} = 1 + \chi^2 - \eta^2$.

Appendix B: The Central Observers

In this section we introduce freely falling "central" observers, the ones that populate the (time-dependent, spherical) boundary separating the two *connected* universes. On each of the embedding diagrams shown in Fig. 5, central observers are represented by a point with $Z = 0$ (the narrowest point of wormhole's neck), while in both standard Kruskal and modified diagrams (Fig. 1) they are represented by the same vertical geodesic, $\chi = 0$, $-1 < \eta < 1$, that runs from past to future singularity. We use the plural mode of description here because, formally, there is an infinite number of central observers differing from each other by their location on the boundary sphere. On the other hand, the Fermi normal coordinates introduced below should be thought of as pertaining to just one, specifically chosen, central observer. Our interest in central observers stems primarily from their simplicity, but also from their potential use for the description of physics in "the central region" (in 't Hooft's terminology [30]) of the extended spacetime manifold.

Let us re-write our metric (17) to quadratic order in Fermi normal coordinates (FNC) [31], $x^{\alpha}_{\mathrm{F}} = (t_{\mathrm{c}}, x^j) \equiv (t_{\mathrm{c}}, x, y, z)$, surrounding a central geodesic, $\mathcal{C}$, defined by the condition $\chi = 0$ (here, t_{c} denotes the proper time measured along the geodesic). The general form of the metric in FNC is

$$g^{\mathrm{F}}_{00} = \eta_{00} - R^{\mathrm{F}}_{0j0k}(t_{\mathrm{c}})\, x^j x^k + \mathcal{O}(x^3), \tag{B1}$$

$$g^{\mathrm{F}}_{0\ell} = -\frac{2}{3} R^{\mathrm{F}}_{0j\ell k}(t_{\mathrm{c}})\, x^j x^k + \mathcal{O}(x^3), \tag{B2}$$

$$g^{\mathrm{F}}_{\ell m} = \eta_{\ell m} - \frac{1}{3} R^{\mathrm{F}}_{\ell jmk}(t_{\mathrm{c}})\, x^j x^k + \mathcal{O}(x^3), \tag{B3}$$

so the task is to find the corresponding curvature components evaluated on $\mathcal{C}$. Since in our case the metric on $\mathcal{C}$ is given by

$$ds^2\big|_{\mathcal{C}} = 4r_\mathrm{s}^2(1-\eta^2)d\eta^2 - \frac{4r_\mathrm{s}^2}{1-\eta^2}d\chi^2 - r_\mathrm{s}^2(1-\eta^2)^2 d\Omega^2, \tag{B4}$$

we have,

$$dt_\mathrm{c} = 2r_\mathrm{s}\sqrt{1-\eta^2}\, d\eta, \tag{B5}$$

which, upon integration, gives the relation between the proper and coordinate time,

$$t_\mathrm{c} = r_\mathrm{s}\left(\eta\sqrt{1-\eta^2} + \arcsin\eta\right) \approx 2r_\mathrm{s}\eta\left(1 - \frac{\eta^2}{6} - \frac{\eta^4}{40}\right), \tag{B6}$$

with observer's total lifetime being

$$t_\mathrm{c}^{(\mathrm{total})} = \pi r_\mathrm{s}. \tag{B7}$$

The choice of an orthonormal frame parallel transported along the geodesic is also straightforward, and, on the basis of Eq. (B4), may be taken to be

$$\hat{e}_{(0)} = \frac{\partial}{\partial t_\mathrm{c}}\bigg|_{\mathcal{C}} = \left(\frac{1}{2r_\mathrm{s}\sqrt{1-\eta^2}}, 0, 0, 0\right), \tag{B8}$$

$$\hat{e}_{(1)} = \frac{\partial}{\partial x}\bigg|_{\mathcal{C}} = \left(0, \frac{\sqrt{1-\eta^2}}{2r_\mathrm{s}}, 0, 0\right), \tag{B9}$$

$$\hat{e}_{(2)} = \frac{\partial}{\partial y}\bigg|_{\mathcal{C}} = \left(0, 0, \frac{1}{r_\mathrm{s}(1-\eta^2)}, 0\right), \tag{B10}$$

$$\hat{e}_{(3)} = \frac{\partial}{\partial z}\bigg|_{\mathcal{C}} = \left(0, 0, 0, \frac{1}{r_\mathrm{s}(1-\eta^2)\sin\Theta}\right). \tag{B11}$$

Then, following the standard prescription for constructing FNC (see [31] for details; also, [17]) and using the results of Appendix A, after some algebra we find,

$$R^\mathrm{F}_{0101} = 2A(\eta), \quad R^\mathrm{F}_{0202} = R^\mathrm{F}_{0303} = -A(\eta), \quad R^\mathrm{F}_{1212} = R^\mathrm{F}_{1313} = A(\eta), \quad R^\mathrm{F}_{2323} = -2A(\eta), \tag{B12}$$

with

$$A(\eta) \equiv \frac{1}{2r_\mathrm{s}^2\left(1-\eta^2\right)^3}, \tag{B13}$$

and, correspondingly,

$$g^\mathrm{F}_{00} = 1 + A\left(y^2 + z^2 - 2x^2\right), \quad g^\mathrm{F}_{11} = -\left[1 + (A/3)\left(y^2+z^2\right)\right], \tag{B14}$$

$$g^\mathrm{F}_{22} = -\left[1 + (A/3)\left(x^2 - 2z^2\right)\right], \quad g^\mathrm{F}_{33} = -\left[1 + (A/3)\left(x^2 - 2y^2\right)\right], \tag{B15}$$

$$g^\mathrm{F}_{12} = g^\mathrm{F}_{21} = (A/3)xy, \quad g^\mathrm{F}_{13} = g^\mathrm{F}_{31} = (A/3)xz, \quad g^\mathrm{F}_{23} = g^\mathrm{F}_{32} = -(2A/3)yz. \tag{B16}$$

The Fermi metric can be written in more compact form by introducing spherical coordinates, $(t_\mathrm{c}, r_\mathrm{c}, \theta, \varphi)$, with the x direction playing the role of the polar axis,

$$y = r_\mathrm{c}\sin\Theta\cos\Phi, \quad z = r_\mathrm{c}\sin\Theta\sin\Phi, \quad x = r_\mathrm{c}\cos\Theta, \tag{B17}$$

resulting in

$$ds^2_\mathrm{F} = \left[1 - Ar_\mathrm{c}^2\left(3\cos^2\Theta - 1\right)\right]dt_\mathrm{c}^2 - dr_\mathrm{c}^2 - \left(1 + Ar_\mathrm{c}^2/3\right)r_\mathrm{c}^2 d\Theta^2 - \left[1 + \left(Ar_\mathrm{c}^2/3\right)\left(3\cos^2\Theta - 2\right)\right]r_\mathrm{c}^2\sin^2\Theta d\Phi^2. \tag{B18}$$

Acknowledgments

The author thanks Sergei Kopeikin and Loris Magnani for stimulating discussions.

[1] M. D. Kruskal, Maximal Extension of Schwarzschild Metric, Phys. Rev. 119, 1743–1745 (1960).
[2] G. Szekeres, On the singularities of a Riemannian manifold, Publ. Math. Debrecen 7, 285–301 (1960).
[3] R. Penrose, Gravitational Collapse and Space-Time Singularities, Phys. Rev. Lett. 14, 57–59 (1965).
[4] R. Penrose, Gravitational Collapse: The Role of General Relativity, Riv. Nuovo Cimento 1, 257 (1969); reprinted in Gen. Relativ. Gravit. 34, 1141–1165 (2002).
[5] A. S. Eddington, A comparison of Whitehead's and Einstein's formulae, Nature 113, 192 (1924).
[6] D. Finkelstein, Past-Future Asymmetry of the Gravitational Field of a Point Particle, Phys. Rev. 110, 965–967 (1958).
[7] C. W. Misner, K. S. Thorne, and J. A. Wheeler, *Gravitation* (W. H. Freeman, San Francisco, 1973).
[8] W. Israel, New Interpretation of the Extended Schwarzschild Manifold, Phys. Rev. 143, 1016–1021 (1966).
[9] J. Ehlers, in *Relativity, Astrophysics and Cosmology*, Proceedings of the Summer School, Banff, Alberta, 1972, edited by W. Israel (Reidel, Dordrecht, 1973).
[10] W. Pajerski and E. T. Newman, Trapped surfaces and the development of singularities, J. Math. Phys. 12, 1929–1937 (1971).
[11] T. Klösch and T. Strobl, Explicit global coordinates for Schwarzschild and Reissner–Nordström solutions, Class. Quantum Grav. 13, 1191–1200 (1996).
[12] C. Fronsdal, Completion and Embedding of the Schwarzschild Solution, Phys. Rev. 116, 778–781 (1959).
[13] W. Rindler, Kruskal Space and the Uniformly Accelerated Frame, Am. J. Phys. 34, 1174–1178 (1966).
[14] J. L. Synge, The Gravitational Field of a Particle, Proc. R. Ir. Acad. Sect. A 53, 83–114 (1950).
[15] W. G. Unruh, Universal coordinates for Schwarzschild black holes, arXiv:1401.3393 [gr-qc].
[16] K. Martel and E. Poisson, Regular coordinate systems for Schwarzschild and other spherical spacetimes, Am. J. Phys. 69, 476–480 (2001).
[17] E. Poisson, *A Relativist's Toolkit: The Mathematics of Black-Hole Mechanics* (Cambridge University Press, Cambridge, 2009).
[18] K. Lake, Maximally extended, explicit and regular coverings of the Schwarzschild–de Sitter vacua in arbitrary dimension, Class. Quantum Grav. 23, 5883–5895 (2006).
[19] K. Lake, Some notes on the Kruskal–Szekeres completion, Class. Quantum Grav. 27, 097001 (2010).
[20] C. Röken, A family of horizon-penetrating coordinate systems for the Schwarzschild black hole geometry with Cauchy temporal functions, Gen. Relativ. Gravit. 54, 33 (2022).
[21] Y. M. Bisson and K. Lake, Israel coordinates for all static spherically symmetric spacetimes with vanishing second Ricci invariant, Phys. Rev. D 108, 104017 (2023).
[22] C. Cederbaum and M. Wolff, Some new perspectives on the Kruskal–Szekeres extension with applications to photon surfaces, Lett. Math. Phys. 114, 40 (2024).
[23] G. Sassi, Analytical Derivation of the Embedding of the Schwarzschild Solution in a Flat Space-Time, Nuovo Cimento B 102, 511–516 (1988).
[24] J. P. S. Lemos and D. L. F. G. Silva, Maximal extension of the Schwarzschild metric: From Painlevé–Gullstrand to Kruskal–Szekeres, Ann. Phys. (N.Y.) 430, 168497 (2021).
[25] A. Einstein and N. Rosen, The Particle Problem in the General Theory of Relativity, Phys. Rev. 48, 73–77 (1935).
[26] R. W. Fuller and J. A. Wheeler, Causality and Multiply Connected Space-Time, Phys. Rev. 128, 919–929 (1962).
[27] L. Flamm, Beiträge zur Einsteinschen Gravitationstheorie, Phys. Z. 17, 448–454 (1916); reprinted in Gen. Relativ. Gravit. 47, 72 (2015).
[28] C. F. Chyba, Time-dependent embeddings for Schwarzschild-like solutions to the gravitational field equations, J. Math. Phys. 23, 1662–1667 (1982).
[29] P. Collas and D. Klein, Embeddings and time evolution of the Schwarzschild wormhole, Am. J. Phys. 80, 203–210 (2012).
[30] G. 't Hooft, Alternative theory for the quantum black hole and the temperature of its quantum radiation, arXiv:2410.16891 [gr-qc] (2024).
[31] F. K. Manasse and C. W. Misner, Fermi Normal Coordinates and Some Basic Concepts in Differential Geometry, J. Math. Phys. 4, 735 (1963).